This is the peer-reviewed, final accepted version for American Mineralogist, published by the Mineralogical Society of America.
The published version is subject to change. Cite as Authors (Year) Title. American Mineralogist, in press.
DOI: https://doi.org/10.2138/am-2022-8138. http://www.minsocam.org/

The Crystal Structure and Chemistry of Natural Giniite and Implications for Mars

Wordcount: 5081

Christopher. T. Adcock[1], Elisabeth M. Hausrath[1], Elizabeth B. Rampe[2], Hexiong Yang[3], and Robert T. Downs[3]

[1]Department of Geoscience, University of Nevada, Las Vegas, 4505 S. Maryland Pky., Las Vegas, Nevada 89154-4010, U.S.A.
[2]NASA Johnson Space Center, 2101 E NASA Pkwy, Houston, TX 77058, U.S.A.
[3]Department of Geosciences, University of Arizona, 1040 East 4th Street, Tucson, Arizona 85721-0077, U.S.A.

REVISION 1

Abstract

Investigations of planetary processes using phosphate minerals often focus on igneous, recrystallized, or potentially metasomatized minerals, likely as a result of the minerals commonly available for study within meteorites and lunar samples. However, Mars is a relatively phosphorus-rich planet and possesses abundant evidence of past aqueous surface interactions. Therefore, secondary phosphate phases may be important on the Martian surface. Giniite [$Fe^{2+}Fe_4^{3+}(PO_4)_4(OH)_2 \cdot 2H_2O$] is a secondary phosphate mineral that has been suggested as a potentially significant phase at locations in Gusev Crater and Meridiani Planum on Mars. Although relatively rare as a natural mineral on Earth, giniite has gained attention as an important mineral in industry and technology, especially the lithium battery industry, and the ferrian version of the mineral is often synthesized. This suggests giniite may be important as an *in-situ* resource utilization (ISRU) target for future extended human missions to Mars. Despite this, there are few data available on the natural mineral and the last characterization of the structure was over 40 years ago. There has also been confusion in the literature as to whether giniite is orthorhombic or monoclinic. In this work we revisit and document the chemistry and crystal structure of natural giniite from the type locality at the Sandamab pegmatite in Namibia

using updated techniques. Our results refine and update what was previously known regarding the structure and chemistry of giniite and support the potential of the mineral as a possible Martian scientific and resource target for further study to aid future missions.

Keywords

Giniite, Fe-phosphate, ferrous giniite, ferric giniite, ferrian, phosphate, hydroxyphosphate, Martian habitability, Mars, ISRU, XRD,

Introduction

The study of phosphorus minerals yields insight into planetary interior and surface processes. For instance, primary or igneous phosphate minerals have been used to investigate volatile abundances in the interiors of Earth, Mars, the Moon, and asteroidal bodies (e.g. McCubbin et al., 2011; Patiño Douce et al., 2011; Filiberto et al., 2016; Jones et al., 2014; McCubbin et al., 2014), as potential indicators of oxygen fugacity during late stage magma crystallization (Shearer et al., 2015), and even as recorders of past aqueous surface environments on Mars (Mojzsis and Arrhenius, 1998; Hurowitz et al., 2006; Ming et al., 2006; Adcock and Hausrath, 2015). Phosphorus, as phosphate or a more reduced species, is also an essential nutrient for all known life, and considered important in prebiotic reactions that led to life on Earth (Wald, 1964; Westheimer, 1987; Powner et al., 2009; Pasek and Kee, 2011; Benner and Kim, 2015; Burcar et al., 2016). Consequently, P-bearing minerals have important implications for past and present habitability and the potential for life on other planetary bodies (Weckwerth and Schidlowski, 1995; Mojzsis et al., 1996; Yang et al., 2011; Adcock et al., 2013; Adcock and Hausrath, 2015).

Investigations of planetary processes using phosphate minerals often focus on igneous, recrystallized, or potentially metasomatized minerals (e.g. Brearley and Jones, 1998; Jones et al., 2014; McCubbin and Jones, 2015; Adcock et al., 2017). For extraterrestrial studies, this focus is likely the result of the minerals commonly available for study within meteorites and lunar samples. Though various secondary phosphate minerals are present in some meteorites (Dyar et al., 2014), the most common phosphate minerals in most meteorites and lunar samples are merrillite [$Ca_9NaMg(PO_4)_7$] and apatite [$Ca_5(PO_4)_3(F,Cl,OH)$], often of igneous origin (Shearer et al., 2006; McCubbin et al., 2014; Adcock and Hausrath, 2015). This is especially the case for Martian meteorites (McSween and Treiman, 1998).

However, Mars is a relatively phosphorus-rich planet (Wänke and Dreibus, 1988; Taylor, 2013) and analyses from the surface of Mars indicate relatively high P-concentrations in soils, rocks, and dust compared to Earth (Goetz et al., 2005; Gellert et al., 2006; Yang and Post, 2011; Rampe et al., 2017; Yen et al., 2017; Rampe et al., 2020). Mars also possesses abundant evidence of past aqueous surface interactions (Carr and Head III, 2003; Hurowitz et al., 2006; Grotzinger et al., 2014; Adcock and Hausrath, 2015; Rampe et al., 2016; McCollom et al., 2018). Reactive transport modeling of measured rock profiles at Gusev Crater indicate dissolution of primary phosphate minerals, the product of which would be secondary phosphates (Adcock and Hausrath, 2015). Thermodynamic modeling by Berger et al., (2016) indicates the formation of the secondary phosphate mineral strengite ($FePO_4 \cdot 2H_2O$) at Gale Crater, Mars. Recent data from the Alpha Particle X-ray Spectrometer (APXS) on board *Curiosity* at Gale Crater indicate enrichments of P and Mn in nodules, veins, and other surface features there (Berger et al., 2021). ChemMin diffraction data from Gale Crater also show the potential presence of secondary flourapatite (Rampe et al., 2017) and a secondary manganese-bearing phosphate of the jahnsite-

whiteite group (Treiman et al., 2021). These models and observations suggest aqueously altered or precipitated secondary phosphate minerals may not be uncommon phases on the Martian surface and thus warrant more in-depth consideration.

Among the potential secondary minerals that may occur on Mars is giniite [$Fe^{2+}Fe^{3+}{}_4(PO_4)_4(OH)_2 \cdot 2H_2O$]. Although rare on Earth, giniite has gained attention in industry, including as a potential component in Li-ion battery production (Hong et al., 2003; Whittingham, 2004; Lv et al., 2017), wastewater processing (Duan et al., 2013; Han et al., 2017; Priambodo et al., 2017), biomedical materials, and as a deprotonation catalyst (Chen et al., 2014; Nedkov et al., 2016).

In comparison to Earth, Mars has notably higher Fe and P content, and Hausrath et al., (2013) first suggested that giniite may be a significant secondary phase on that planet based on terrestrial hydrothermal experiments that produced giniite, and Mössbauer data acquired from Gusev Crater on Mars. In later work, alteration experiments using P-enriched basalts as analogs of rocks at Meridiani Planum also produced giniite, suggesting the mineral may likewise be of importance at that location on Mars (McCollom et al., 2018). The confirmation of giniite on Mars would be scientifically important. Like primary minerals, secondary minerals are products of their formation environments, and are therefore potentially useful indicators of past Martian environmental conditions (e.g. Klingelhöfer et al., 2004; Wiseman et al., 2008). Minerals like giniite also have implications for the availability of bio-essential phosphate in these past environments, and thus are astrobiologically relevant. Giniite may further represent a potential resource for extended human missions to Mars. For instance, as a hydrated mineral, giniite contains approximately 48 liters of H_2O per metric ton (not including the OH^- component) that can be driven off between 175° and 300° C (Jambor and Dutrizac, 1988; Rouzies et al., 1994;

Gonçalve et al., 2017; Liu et al., 2017). McCollom et al., (2018) suggest as much as 8% of the Fe in the Burns Formation at Meridiani Planum on Mars may be held in giniite, with another 29% in jarosite (a hydrated Fe-sulfate holding ~10% H_2O) (Morris et al., 2006). Therefore, giniite, along with other hydroxides in Martian soils or rocks, could be a useful source of water. The mineral could also be processed into fertilizer, and oxidation of the Fe^{2+} component in minerals has been shown to produce H_2 or CH_4, potential fuel components (e.g. Miller et al., 2017; Adcock et al., 2021). In Situ Resource Utilization (ISRU) is the practice of using materials or energy sources derived at space destinations (such as Mars) to replace or supplement resources that would otherwise have to be transported from Earth (Sanders and Larson, 2011; Sridhar et al., 2000; Starr and Muscatello, 2020). The above qualities, including the potential availability, suggest that giniite may be a good subject for further investigation as a possible Martian ISRU target.

Despite the potential importance of giniite both terrestrially and on Mars, most of the research and data currently available focus upon the synthetic, generally ferrian, analog of the mineral, rather than the natural, typically more reduced form. To our knowledge, there are few data on the natural mineral and the only characterization was over 40 years ago by Keller (1980a; 1980b), who originally documented the mineral with X-ray diffraction, electron microprobe and thermogravimetric analysis (TGA). The original structure was reported as orthorhombic (Fleischer et al., 1980; Keller, 1980a), but following work suggested this assessment was the result of twinning and the structure was revised to monoclinic (Keller, 1980b). Despite this, giniite is still sometimes reported as orthorhombic (e.g. Liu et al., 2017; Zhang et al., 2013). In this work we use modern single-crystal X-ray diffraction with an area detector on natural giniite from the type locality, to reassess the structure in the correct monoclinic system. Additionally, Raman

spectroscopy and electron microprobe techniques are employed to revisit and document the chemistry.

Background

Minerals exhibit characteristics of their formation environments. In the case of secondary phosphate minerals, these characteristics may include temperature, pH, chemistry, and oxidation state of any interacting fluids (Moore, 1973; Hawthorne, 1998; Dill et al., 2008). Vivianite [$Fe_3^{2+}(PO_4)_2 \cdot 8H_2O$] for instance, indicates a near neutral pH, anoxic, reducing, low temperature, high water:rock ratio aqueous formation environment (Hawthorne, 1998; McGowan and Prangnell, 2006). Brushite [$Ca(HPO_4) \cdot 2H_2O$] and monetite [$Ca(HPO_4)$] are indicators of acidic, and potentially biogenic formation environments on Earth (Dumitras et al., 2004; Dosen and Giese, 2011; Frost and Palmer, 2011; Frost et al., 2013b). Although not confirmed on Mars, brushite has been suggested as a possible acidic weathering product on that planet (Hurowitz et al., 2006; Ming et al., 2006). Secondary Al- and Fe-phosphates are also probable components in the P-enriched amorphous fraction of soils documented at Gale Crater by the Mars Science Laboratory *Curiosity,* again with implications for past aqueous Martian weathering environments (Morris et al., 2013; Tu et al., 2014; Vaniman et al., 2014; Rampe et al., 2016). All of these secondary phosphate minerals have the potential to inform us about past and present formation environments, including those on Mars.

Giniite is no exception and its presence and paragenesis can provide detailed insights regarding its formation environment. On Earth, the mineral typically occurs within pegmatites or iron-bearing ore bodies (Keller, 1980a; Jambor and Dutrizac, 1988; Nunes et al., 2009). In pegmatite settings, the mineral is a product of hydrothermal alteration of primary triphylite

[$LiFePO_4$]. Keller (1980a) identified it as part of a paragenetic or age sequence of triphylite → hureaulite → [an unidentified dark green mineral + giniite] → tavorite → leukophosphite. Keller (1980a) speculated that giniite took the place of barbosalite [$Fe^{2+}Fe^{3+}{}_2(PO_4)_2(OH)_2$] in a similar sequence at other pegmatites in the region (e.g. Keller and Knorring, 1989), suggesting giniite is the product of mid- to late-stage hydrothermal alteration (<250 °C) (Hawthorne, 1998).

In metal ore bodies the genetic history of giniite is less clear. Phosphorus is a common impurity in iron-bearing metal ore bodies (Cheng et al., 1999; Delvasto et al., 2008; Ofoegbu, 2019), and at the Silver Coin mine in Nevada, USA, phosphate minerals, including giniite, are products of acidic hydrothermal precipitation associated with the ore body (Adams et al., 2015). However, at mines near Saalfeld, Germany, giniite appears to occur as a low temperature weathering product of the ore body associated with a hydrous mineral gel formed in open natural caves (Ullrich, 2017).

Recent industrial, technologic, and scientific interests in the mineral (noted above) have led to several synthesis methods and studies. Most of these synthesis methods produce a fully ferric form of the mineral we refer to as ferrian giniite [$Fe^{3+}{}_5(PO_4)_4(OH)_3 \cdot H_2O$] (e.g. Jambor and Dutrizac, 1988; Rouzies et al., 1994; Frost et al., 2007; Duan et al., 2013; Zhang et al., 2013; Nedkov et al., 2016; Han et al., 2017; Liu et al., 2017). However, mixed Fe valence giniite more similar to natural giniite has also been synthesized with ferrous/ferric content up to $Fe^{2+}{}_{1.7}/Fe^{3+}{}_{3.3}$ (Rouzies et al., 1994). To account for different Fe^{2+}/Fe^{3+} ratios, charge balance is maintained by changes in the OH^-/ H_2O ratio through hydrating/dehydrating OH^- sites (Keller, 1980a; Rouzies et al., 1994) and can be expressed as

$$[Fe^{2+}{}_x\, Fe^{3+}{}_{(5-x)}(PO_4)_4(OH)_{(3-x)} \cdot (1+x)H_2O].$$

It is of note, however, that in the absence of measured data, giniite is often reported with 2 H_2O

units regardless of Fe valence or OH^- content (e.g. Roncal-Herrero et al., 2009; Zhang et al., 2015; Priambodo et al., 2017). In addition, x=1.7 is the highest Fe^{2+} content currently observed. Corbin et al., (1986) synthesized a fully ferrous phase [Fe_5^{2+} $P_4O_{20}H_{10}$, or Fe_5^{2+} $H_2(PO_4)_4 \cdot 4H_2O$] (i.e., x=5) referred to as giniite (e.g. Dyar et al., 2014; Gonça ves et al., 2017). However, a fully ferrous giniite structure is not stable, and instead this chemistry adopts the hureaulite structure [$Mn_5(PO_3OH)_2(PO_4)_2 \cdot 4H_2O$] (Corbin et al., 1986).

Although the rare natural occurrence of giniite on Earth somewhat limits paragenetic and minerogenetic data, the conditions of giniite synthesis can yield further insight into the environments where the mineral may form. Based on synthesis methods, giniite forms under relatively high water:rock ratios (>10:1) and formation temperatures from 25° to 250°C (>150°C appearing optimum for highest yields) (Rouzies et al., 1994; Roncal-Herrero et al., 2009; Hausrath et al., 2013; Nedkov et al., 2016; Gonça ves et al., 2017). Highly acidic conditions appear to be optimum (pH 0.6 to 2) (Jambor and Dutrizac, 1988; Hausrath et al., 2013). However, in the presence of other monovalent cations like Na and K, giniite can form at as high as pH 6 (Gonça ves et al., 2017). While these conditions represent a range of potential settings for giniite formation, the mineral can exhibit variable chemistry and morphology while maintaining the giniite structure (Jambor and Dutrizac, 1988; Zhang et al., 2013) and these aspects may reflect specific details of formation conditions. For instance, Roncal-Herrero (2009) found that crystal morphology of giniite synthesized at 150°C was spheroidal while giniite synthesized at 200°C had a bi-pyramidal morphology. Other studies have noted morphology dependencies based on solution Fe and P concentrations (dendritic, spherical, and octahedral) (Liu et al., 2017), and the presence of different organic compounds in synthesis solutions (spheres and star-like) (Duan et al., 2013; Han et al., 2017). Tubular morphologies have been

reported as products of biogenic formation at 25°C (Nedkov et al., 2016). The pH and presence of Li, Na, or K in solution also appear to act on morphology (asterisk- or flower-like, and dendritic morphologies) (Gonça ves et al., 2017). It is not clear if the Li, Na, or K substitute into giniite in that study, however SO_4^{2-} substitution for PO_4^{3-} has been noted (Jambor and Dutrizac, 1988) and divalent cations including Mn and Mg are known to incorporate into the mineral (Keller, 1980a). These conditions, though potentially broader, are not inconsistent with what is known about natural giniite formation environments.

Although giniite has not been definitively identified on Mars, several lines of evidence suggest that it may be present. Experiments that mimic Martian conditions of acidic solutions placed in contact with a mixture of fluorapatite, olivine, and basaltic glass at 150°C by Hausrath et al. (2013) produced ferrian giniite [$Fe_5(PO_4)_4(OH)_3 \cdot 2H_2O$]. Follow-up Mössbauer measurements of the ferrian giniite alteration products were consistent with analyses performed by the Mars Exploration Rover *Spirit* on Paso Robles soil at Gusev Crater. Hausrath et al. (2013) could not confirm the phase on Mars based on Mössbauer alone, as measurements were also consistent with ferric sulfate phases (Hausrath et al., 2013; Dyar et al., 2014). However, Fe_2O_3 + FeO concentrations in PasoRobles and PasoLight1 soils on Mars are too high to be accounted for solely by sulfate phases and indicate acid fluid transport in high fluid:rock ratios to the location of the Paso Robles soils, general conditions shown to precipitate giniite. McCollom et al. (2018) also suggested giniite may help explain phosphate immobility in the Burns formation at Endurance Crater, as well as the potentially high P measured in alteration halos around fractures previously documented in the Stimson and Murray formations at Gale Crater suggesting the presence of phosphate-rich fluids (Yen et al., 2017). The P-containing fluids that formed these alteration haloes have also been quantitatively modeled (Hausrath et al., 2018). Rampe et al.

(2017), suggest acidic phosphate-rich fluids in the lower Murray at Gale Crater. This indicates conditions suitable for the natural formation of giniite, especially considering giniite genesis at the Silver Coin Mine, Nevada. Therefore, formation of giniite or other ferric phosphate phases may have occurred at multiple locations on Mars. Updating and refining our fundamental knowledge of these minerals, and investigating them more deeply, will help us to detect and identify them on the Martian surface.

Experimental

Materials

A natural sample of giniite was acquired from the Sandamab pegmatite, Namibia by the RRUFF project (Lafuente et al., 2016). Sandamab (sometimes spelt Sandamap) pegmatite is the type locality for the mineral as originally identified by Keller (1980a; 1980b). The sample was a black fragment within a more massive sample of associated triphylite, hureaulite, yellow-greenish tavorite, and black heterosite and was preliminarily identified as giniite based on color and rough habit. RRUFF reference number is R060765 (Supplementary Figure S1).

Analytical Methods

The broad scan Raman spectrum of giniite was collected from a randomly oriented crystal with a Thermo Almega microRaman system using a solid-state laser with a frequency of 532 nm at 150 mW and a thermoelectrically cooled CCD detector. The laser is partially polarized with 4 cm^{-1} resolution and a spot size of 1 μm.

Chemical analyses were carried out on a Cameca SX-100 electron microprobe (EMP). The giniite sample was mounted in epoxy, polished and carbon coated. Samples were analyzed

using wavelength-dispersive spectroscopy (WDS) X-ray analysis. Analysis conditions were 15 keV and 10 nA using a 2 μm beam. Standards and configuration package are detailed in Supplementary Table S1. Multiple analyses (n=15, Figure 1) of the giniite crystal were taken and averaged. EMP does not detect OH-, H_2O, or Fe valence. To estimate OH^- and H_2O, ideal stoichiometry as determined by Keller (1980a) of $Fe^{2+}Fe^{3+}{}_4(PO_4)_4(OH)_2 \cdot 2H_2O$ was used. To estimate the Fe valence ratio, the EMP data were fit to the ideal formula with $Fe^{3+} = 4$ formula units. Synthetic giniite is known to have variable Fe valence and this may be possible for natural giniite as well. Therefore, the EMP data were further fit to a range of stoichiometries based on $Fe^{2+}{}_x\, Fe^{3+}{}_{(5-x)}(PO_4)_4(OH)_{(3-x)} \cdot (1+x)H_2O$ (Keller, 1980; Rouzies et al., 1994) by varying x to determine the Fe^{3+} formula units and calculating the resulting Fe^{2+} formula units and the estimated OH^- and H_2O. A "best fit" was determined based on total Fe and PO_4 formula units being closest to the ideal of 5 and 4 respectively, in the same fit.

Single-crystal X-ray diffraction (SC-XRD) of giniite was carried out using Mo*Kα* radiation on a Rigaku XtaLAB Synergy diffractometer and radiation at 50 kV and 1mA. All reflections were indexed on the basis of a monoclinic unit-cell (Table 1, Supplementary Table S2). The systematic absences of reflections suggested the possible space group *Pn*, or *P*2/*n*. The crystal structure was solved and refined using SHELX2018 (Sheldrick, 2015a; Sheldrick, 2015b) based on space group *P*2/*n*, because it yielded better refinement statistics in terms of bond lengths and angles, atomic displacement parameters, and *R* factors. All H atoms were located from the difference Fourier maps. The ideal chemistry was assumed during the refinements. The positions of all atoms were refined with anisotropic displacement parameters, except those for the H atoms, which were refined only with isotropic parameters.

Results

Structure

X-ray diffraction data collected in this study allowed calculation of a powder X-ray diffraction pattern that is a very close match to published patterns of both a synthetic ferric giniite (Frost et al., 2007) and Keller's (1980a) natural giniite sample (Figure 2). The close match suggests the study sample is indeed giniite. Final coordinates and displacement parameters of atoms in giniite are listed in Supplementary Table S3, and selected bond distances in Table 2. Calculated bond-valence sums using the parameters of Brese and O'Keeffe (1991) are given in Table 3. Crystallographic results of the single crystal data indicate giniite is monoclinic $P2/n$, a = 10.3472(6), b = 5.1497(2), c = 14.2338(7) Å, β = 111.175(6)° and V = 707.24(7) Å^3 (Table 1 and Supplementary Table S2). Atomic positions in Supplementary Table S3 show three unique Fe sites (here labeled Fe1, Fe2 and Fe3) and two unique PO_4 sites (P1 and P2), as well as O and H positions. Determined Fe-O and P-O bond length values fall within expected ranges (Gagné and Hawthorne, 2018; Kanowitz and Palenik, 1998) with average (Fe1-O) bond lengths (2.14 Å) longer than the other two (2.01 Å) indicating that Fe1 contains Fe^{2+} while Fe2 and Fe3 contain Fe^{3+} (Table 2). Bond valence calculations are consistent with this assignment and are generally as expected (Table 3) with the potential exception of the O7 site which is ~0.45 deficient.

Chemistry

Results of 15 EMP analyses (Figure 1 and Supplementary Table S4) were averaged into a single analysis which appears in Table 4 along with Keller's (1980a) original EMP analysis. Low analysis totals are the result of unaccounted for OH^- and molecular water which the technique cannot directly detect. EMP can also not detect Fe valence state. In order to estimate wt% OH^-, H_2O, and Fe^{2+}/Fe^{3+} for comparison to Keller (1980a), the analyses from this study and Keller

(1980a) were fit to the ideal giniite formula of $Fe^{2+}Fe^{3+}{}_4(PO_4)_4(OH)_2 \cdot 2H_2O$ with Fe^{3+}=4.00. This fitting produced an average stoichiometry of $(Fe^{2+}{}_{0.80}Mn_{0.11}Mg_{0.02})_{\Sigma=0.93}Fe^{3+}{}_{4.00}(PO_4)_{4.03}(OH)_{2.00}\cdot 2H_2O$ for this study and $(Fe^{2+}{}_{0.67}Mn_{0.07}Mg_{0.13})_{\Sigma=0.87}Fe^{3+}{}_{4.00}(PO_4)_{4.05}(OH)_{2.00}\cdot 2H_2O$ for Keller (1980a) data. Incorporating the estimates as wt.% into the EMP data improved the analysis totals for this study and Keller (1980a) to ~97.15 and 91.83 wt% respectively (Table 4).

EMP data fit to a range of Fe valence ratios based on $[Fe^{2+}{}_x\, Fe^{3+}{}_{(5-x)}(PO_4)_4(OH)_{(3-x)} \cdot (1+x)H_2O]$ (Keller, 1980; Rouzies et al., 1994), with x used to determine the Fe^{3+} valence (i.e. Fe^{2+} was calculated), produced a "best fit" stoichiometry of $(Fe^{2+}{}_{0.90}Mn_{0.11}Mg_{0.02})_{\Sigma=1.03}Fe^{3+}{}_{3.92}(PO_4)_{4.05}(OH)_{1.92}\cdot 2.08H_2O$ (Supplementary Tables S5 and S6). This fit is based on x = 1.08 to determine Fe^{3+}, however, the calculated Fe^{2+} is 1.03 formula units.

A broad scan Raman spectrum in Figure 3 is consistent with previously reported giniite spectra. There is one non-equivalent hydroxyl group and one water molecule with two non-equivalent O-H pairs in giniite, consistent with the single sharp peak at 3324 cm^{-1} that overlaps with the broad peak at ~3250 cm^{-1}, typical of overlapping O-H stretching modes for OH and H_2O (e.g. Frost et al., 2011; Kolesov, 2006; Weber et al., 2018). PO_4 symmetric stretching modes are in the 800 – 1100 cm^{-1} range with asymmetric ν_3 stretching in the 1100 to 1200 cm^{-1} range. In phosphates, bands in the 400 – 650 cm^{-1} range are generally representative of O-P-O angle bending (both ν_2 and ν_4) (Frost et al., 2007; Hausrath and Tschauner, 2013). The sharp bands in the 200 – 440 cm^{-1} range are typical of Fe-O stretches (Aatig et al., 2016; Frost et al., 2007, 2013a,c). For a plot of raw data, see Supplementary Figure S2.

Discussion

Minerals like giniite are a challenge to chemically characterize. They contain both ferric and ferrous iron as well as OH^- and H_2O. These components are often undetectable or undistinguishable by common analytical techniques, including electron microprobe. As a result, Keller (1980a) noted low EMP totals for giniite (Table 4) in that study. Using EMP and X-ray data, Keller was able to produce a generalized formula for giniite accounting for the OH/H_2O which can be expressed as

$$Fe^{2+}_{x}\ Fe^{3+}_{(5-x)}\ (PO)_4(OH)_{(3-x)} \cdot (1+x)(H_2O)$$

Thermo-gravimetric analysis allowed Keller (1980a) to estimate water content and thereby conclude "x" in the expression to be 1 which produced an Fe^{3+}: Fe^{2+}+Fe^{3+} formula unit ratio of 0.80 (i.e., $Fe^{2+}/Fe^{3+}{}_4$). Thus, $Fe^{2+}Fe^{3+}{}_4(PO)_4(OH)_2 \cdot 2H_2O$ was accepted as the ideal formula for giniite by the International Mineralogical Association (IMA).

In the present study, Raman data, which are generally consistent with data from a previously characterized synthetic ferric giniite sample (Frost et al., 2007), confirm OH/H_2O in the study sample. EMP analyses from this study, fit to the ideal formula by fixing $Fe^{3+} = 4$ formula units, generate an Fe^{3+}: Fe^{2+}+Fe^{3+} formula unit ratio of ~0.80 and calculated stoichiometry even closer to the ideal formula than Keller's original work fit in the same way (Supplementary Table S5). Like Keller (1980a), the original EMP analyses here produced low totals. However, accounting for the Fe valence and OH/H_2O produces totals of ~97% (Table 4). An additional stoichiometric best fit with the EMP data using the more generalized formula of giniite [$Fe^{2+}_{x}\ Fe^{3+}_{(5-x)}\ (PO)_4(OH)_{(3-x)} \cdot (1+x)(H_2O)$] also produces an Fe^{3+}: Fe^{2+}+Fe^{3+} formula unit ratio of ~0.80 (i.e., $Fe^{2+}{}_{1.03}/Fe^{3+}{}_{3.92,}$ or $x \sim 1$) (Supplementary Table S6). Thus, chemical data in this study are consistent with Keller (1980a) and the ideal giniite formula.

It is of note, however, that in determining the ideal formula for giniite, Keller (1980a) assumed the divalent site stoichiometry to be a fixed integer. A number of studies have documented synthetic giniite with Fe^{3+}: Fe^{2+}+Fe^{3+} ratios ranging from 1 (ferrian giniite) to as low as 0.65 (e.g. Rouzies et al., 1994; Roncal-Herrero et al., 2009; Duan et al., 2013; Gonçalve et al., 2017; Priambodo et al., 2017). Consequently, Fe^{2+} is observed to range from 0 to 1.7 formula units while still maintaining the giniite structure. In fact, one of the interesting aspects of giniite is the range of chemistry, and even morphology, that the mineral can possess while still maintaining the giniite structure (e.g. Jambor and Dutrizac, 1988; Zhang et al., 2013; Gonça ves et al., 2017; Martins et al., 2020). Some of this range can be attributed to analytical uncertainty. Data in this study, for instance, allow for variation in the Fe^{3+}: Fe^{2+}+Fe^{3+} ratio of 0.81 to 0.76 (Fe^{2+} content of 1.0 to 1.2) before the summed Fe or PO_4 stoichiometry begin to deviate too far from giniite. However, the observed range in the literature is too large to be explained by this uncertainty alone. While these variations occur in synthetic forms of giniite, and this study focuses on a natural sample as would be found on Mars, the synthesis conditions of at least some of the giniite discussed here are similar to the known petrogenetic/minerogenetic conditions of natural giniite in both pegmatite and ore body settings. Therefore, though the data in this study are consistent with the ideal Fe^{3+}: Fe^{2+}+Fe^{3+} ratio of 0.80 inferred by Keller (1980a), this ratio may only be nominally true in natural specimens.

Crystallographically, Keller (1980a) originally reported giniite as orthorhombic and this was how it was initially documented as a new mineral (Fleischer et al., 1980). Follow-up work by Keller (1980b) showed that the orthorhombic determination was a probable consequence of unrecognized twinning, and the natural mineral was actually monoclinic. However, synthetic giniite has still been reported as orthorhombic (e.g. Liu et al., 2017; Zhang et al., 2013), possibly

as a product of confusion from the literature. Single crystal data/refinement results in this study of natural giniite indicate our sample to be monoclinic, consistent with Keller (1980b).

The giniite structure can be described as short chains (Fe1-Fe2-Fe1 trimers) of face-sharing irregular FeO_6 octahedra oriented along [100], corner-linked by both 6-coordinated evenly spaced FeO_6 octahedra associated with Fe3 arranged in columns along [010], and alternating $(P1)O_4$ and $(P2)O_4$ tetrahedra (Figure 4). In the context of this description the Fe1 site houses the ferrous iron component. The O atom of the H_2O molecule is bonded to ferric Fe3 and ferrous Fe1 atoms. The O atom in the OH group is bonded to all three Fe atoms and, with H, it is tetrahedrally coordinated (Figure 4). The structure shares some similarities with that of barbosalite $[Fe^{2+}Fe^{3+}{}_2(PO_4)_2(OH)_2]$ (Poienar et al., 2020; Redhammer et al., 2000) which also has Fe trimers joined to phosphate and an additional Fe octahedral site, although in that mineral the trimer valences are ordered Fe^{3+}, Fe^{2+}, Fe^{3+}, whereas in giniite the trimers are sequenced Fe^{2+}, Fe^{3+}, Fe^{2+}. These similarities are in-line with speculation by Keller (1980a) that giniite shares certain structural components with other Fe-hydroxy-phosphates and that in more generalized pegmatitic settings giniite may take the place of barbosalite in the evolution of secondary minerals associated with the decomposition of triphylite.

Of further interest in this study is the "O7" site associated with the Fe1 and P2 sites. Fe-O and P-O bond lengths and bond valence calculations are generally as expected (Tables 2 & 3). However, bond valence sums for the O7 site are deficient (~1.5 e). Non-ideal bond valence sums can result for many reasons, including vacancies or undetected substitutions/components in the structure. In this study, the configuration of the O7 sites results in them being adjacent across an opening in the giniite structure (Figure 4, Supplementary Figure S3). The Fe1-O7-P2 bond angle is 127.33° and the O7-O7 distance is approximately 2.46 Å. It may be possible that H^+ protons

occupy some of these "O7 voids" oscillating between O7 sites, and a shared H^+ proton would account for the valence value. Proton oscillation or "hopping" between sites has previously been indicated in the Fe-phosphate minerals barbosalite [$Fe^{2+}Fe^{3+}{}_2(PO_4)_2(OH)_2$] and ludlamite [$(Fe,Mn,Mg)_3(PO4)_2 \cdot 4H_2O$] where H^+ ions have been suggested to oscillate between OH sites and PO_4 (Frost et al., 2013a,c). Many analytical techniques cannot detect H^+, and for techniques that can, because there is already significant OH^- or H_2O in giniite, it is unlikely such additional H^+ would be easily identified. If undetected H^+ resides in the "O7 void", this may explain the bond valence deficiency and add to the interesting nature of the mineral.

Giniite has gained recent attention in industry and as a potential mineral occurring on Mars. The characteristic of the mineral to maintain the giniite structure and chemistry while exhibiting different morphologies based on formation environment mean it could be a powerful indicator of past environments and potentially of life, on Earth or Mars. Overall, the results of this study refine and better detail the structure of giniite and confirm that giniite is indeed a monoclinic mineral rather than orthorhombic. The results here are also consistent with the ideal formula, including the Fe valence ratio, for natural giniite. However, based on synthetic giniite, variations in the Fe valence ratio cannot be ruled out in the natural mineral, and this should be further investigated in the future. Along with morphology, the Fe valence ratio may be an indicator of formation conditions. In addition, if considering giniite as a potential Martian resource, valence can influence how, and how much, water and H^+ can be evolved from the mineral.

Raman spectrometers, like the spectrometers on the SuperCam and Scanning Habitable Environments with Raman & Luminescence for Organics & Chemicals (SHERLOC) instrument suites on *Perseverance*, X-ray diffractometers, like the CheMin instrument on *Curiosity*, and the

Mössbauer instruments carried by *Spirit* and *Opportunity* all have the potential to identify giniite in situ. This is especially the case if a combination of these instruments is deployed. We encourage deployment of these mineralogical instruments on future Mars missions with data libraries that include secondary phosphates to help identify minerals like giniite that can elucidate habitability and potentially be used as a resource.

Implications

Giniite has become a recent mineral of interest as a potential component in applications including water purification, energy storage, and bio-medical materials on Earth. However, secondary phosphate minerals, like giniite, are also likely to hold a wealth of information regarding past Martian surface processes and past environments. If confirmed on Mars, the variable morphologies and broad formation conditions of giniite may make the mineral especially important as an indicator of past environments and habitably. The discovery of giniite with tubular morphologies on Mars, or in samples returned from Mars, might also be an indicator of past life on the planet. In addition, terrestrial investigations of giniite as a resource in technology and industry have potential implications for Mars. If substantial amounts of giniite are present on Mars, long-term human exploration missions to the planet may be able to utilize the mineral in applications developed on Earth (e.g., water purification, energy storage, bio-medical materials). Beyond this, giniite is also potentially a resource for phosphate, water, and fuel generation on Mars.

Deepening our knowledge base of secondary minerals that are possible or probable on the Martian surface, like giniite, will enhance our resource flexibility during long-term missions on Mars while also yielding insight into the Martian past. Secondary phosphate minerals in samples potentially collected by the *Perseverance* rover and returned by future missions will further our

knowledge of ancient aqueous environments on Mars, their habitability, and potential resources for future human missions. However, if minerals like giniite are to be fully explored as scientific and practical resources, up to date fundamental data, like those provided in this study, are essential.

Acknowledgements

We would like to acknowledge the RRUFF project for data and sample access to the giniite used in this study.

References Cited

Aatiq, A., Tigha, M.R., Fakhreddine, R., Bregiroux, D., and Wallez, G. (2016) Structure, infrared and Raman spectroscopic studies of newly synthetic $A^{II}(Sb^{V}_{0.50}Fe^{III}_{0.50})(PO_4)_2$ (A = Ba, Sr, Pb) phosphates with yavapaiite structure. Solid State Sciences, 58, 44-54.

Adams, P.M., Wise, W.S., and Kampf, A.R. (2015) The Silver Coin Mine. The Mineralogical Record, 45(September–October), 702-728.

Adcock, C.T., and Hausrath, E.M. (2015) Weathering Profiles in Phosphorus-Rich Rocks at Gusev Crater, Mars, Suggest Dissolution of Phosphate Minerals into Potentially Habitable Near-Neutral Waters. Astrobiology, 15, 1060-1075.

Adcock, C.T., Hausrath, E.M., and Forster, P.M. (2013) Readily available phosphate from minerals in early aqueous environments on Mars. Nature Geoscience, 6, 824-827.

Adcock, C.T., Tschauner, O., Hausrath, E.M., Udry, A., Luo, S., Cai, Y., Ren, M., Lanzirotti, A., Newville, M., and Kunz, M. (2017) Shock-transformation of whitlockite to merrillite and the implications for meteoritic phosphate. Nature communications, 8(1), 1-8.

Adcock, C., Hausrath, E., Rampe, E., Panduro-Allanson, R., and Steinberg, S. (2021) In Situ Resources from Water-Rock Interactions for Human Exploration of Mars. In LPI, Ed. 52nd Lunar and Planetary Science Conference, p. 1665. LPI, Virtual.

Benner, S.A., and Kim, H.-J. (2015) The case for a Martian origin for Earth life. Instruments, Methods, and Missions for Astrobiology XVII, 9606, 96060C. International Society for Optics and Photonics.

Berger, J., Schmidt, M., Izawa, M., Gellert, R., Ming, D., Rampe, E., VanBommel, S., and McAdam, A. (2016) Phosphate stability in diagenetic fluids constrains the acidic

alteration model for lower Mt. Sharp sedimentary rocks in Gale crater, Mars. 47th Lunar and Planetary Science Conference, p. 1652. LPI, The Woodlands.

Berger, J., VanBommel, S., Clark, B., Gellert, R., House, C., King, P., McCraig, M., Ming, D., O'Connell-Cooper, C., and Schmidt, M. (2021) Manganese-and Phosphorus-Rich Nodules in Gale Crater, Mars: APXS Results from the Groken Drill Site. In LPI, Ed. 52nd Lunar and Planetary Science Conference, p. 2194. LPI, Virtual.

Brearley, A., and Jones, R. (1998) Chondritic Meteorites. In J. Papike, Ed. Planetary materials, 36, p. 3-1. Reviews in Mineralogy and Geochemistry, Mineralogical Society of America, Chantilly, Virginia.

Brese, N., and O'keeffe, M. (1991) Bond-valence parameters for solids. Acta Crystallographica Section B: Structural Science, 47(2), 192-197.

Burcar, B., Pasek, M., Gull, M., Cafferty, B.J., Velasco, F., Hud, N.V., and Menor-Salván, C. (2016) Darwin's warm little pond: a one-pot reaction for prebiotic phosphorylation and the mobilization of phosphate from minerals in a urea-based solvent. Angewandte Chemie International Edition, 55(42), 13249-13253.

Carr, M.H., and Head III, J.W. (2003) Oceans on Mars: An assessment of the observational evidence and possible fate. Journal of Geophysical Research: Planets, 108(E5), 5042

Chen, Q., Wei, C., Zhang, Y., Pang, H., Lu, Q., and Gao, F. (2014) Single-crystalline hyperbranched nanostructure of iron hydroxyl phosphate $Fe_5(PO_4)_4(OH)_3{\cdot}2H_2O$ for highly selective capture of phosphopeptides. Scientific Reports, 4(1), 1-7.

Cheng, C.Y., Misra, V.N., Clough, J., and Muni, R. (1999) Dephosphorisation of western australian iron ore by hydrometallurgical process. Minerals Engineering, 12(9), 1083-1092.

Corbin, D., Whitney, J., Fultz, W., Stucky, G., Eddy, M., and Cheetham, A. (1986) Synthesis of open-framework transition-metal phosphates using organometallic precursors in acidic media. Preparation and structural characterization of $Fe_5P_4O_{20}H_{10}$ and $NaFe_3P_3O_{12}$. Inorganic Chemistry, 25(14), 2279-2280.

Delvasto, P., Valverde, A., Ballester, A., Muñoz, J.A., González, F., Blázquez, M.L., Igual, J.M., and García-Balboa, C. (2008) Diversity and activity of phosphate bioleaching bacteria from a high-phosphorus iron ore. Hydrometallurgy, 92(3), 124-129.

Dill, H.G., Melcher, F., Gerdes, A., and Weber, B. (2008) The origin and zoning of hypogene and supergene Fe–Mn–Mg–Sc–U–REE phosphate mineralization from the newly discovered Trutzhofmühle aplite, Hagendorf pegmatite province, Germany. The Canadian Mineralogist, 46(5), 1131-1157.

Dosen, A., and Giese, R.F. (2011) Thermal decomposition of brushite, CaHPO4· 2H2O to monetite CaHPO4 and the formation of an amorphous phase. American Mineralogist, 96(2-3), 368-373.

Duan, X., Li, D., Zhang, H., Ma, J., and Zheng, W. (2013) Crystal-Facet Engineering of Ferric Giniite by Using Ionic-Liquid Precursors and Their Enhanced Photocatalytic Performances under Visible-Light Irradiation. Chemistry–A European Journal, 19(22), 7231-7242.

Dumitras, D.-G., Marincea, S., and Fransolet, A.-M. (2004) Brushite in the bat guano deposit from the" dry" Cioclovina Cave (Sureanu Mountains, Romania). Neues Jahrbuch fur Mineralogie-Abhandlungen, 180(1), 45-64.

Dyar, M.D., Jawin, E.R., Breves, E., Marchand, G., Nelms, M., Lane, M.D., Mertzman, S.A., Bish, D.L., and Bishop, J.L. (2014) Mössbauer parameters of iron in phosphate minerals: Implications for interpretation of martian data. American Mineralogist, 99(5-6), 914-942.

Filiberto, J., Gross, J., and McCubbin, F.M. (2016) Constraints on the water, chlorine, and fluorine content of the Martian mantle. Meteoritics & Planetary Science, 51(11), 2023-2035.

Fleischer, M., Cabri, L., Chao, G., and Pabst, A. (1980) New Mineral Names. American Mineralogist, 65, 1065 - 1070.

Frost, R.L., and Palmer, S.J. (2011) Thermal stability of the 'cave'mineral brushite $CaHPO_4 \cdot 2H_2O$–Mechanism of formation and decomposition. Thermochimica Acta, 521(1-2), 14-17.

Frost, R.L., Wills, R.-A., and Martens, W.N. (2007) A Raman spectroscopic study of synthetic giniite. Spectrochimica Acta Part A: Molecular and Biomolecular Spectroscopy, 66(1), 42-47.

Frost, R.L., Bahfenne, S., Čejka, J., Sejkora, J., Plášil, J., Palmer, S.J., Keeffe, E.C., and Němec, I. (2011) Dussertite $BaFe^{3+}{}_3(AsO_4)_2(OH)_5$—a Raman spectroscopic study of a hydroxy-arsenate mineral. Journal of Raman Spectroscopy, 42(1), 56-61.

Frost, R.L., Xi, Y., López, A., Scholz, R., de Carvalho Lana, C., and e Souza, B.F. (2013a) Vibrational spectroscopic characterization of the phosphate mineral barbosalite $Fe^{2+}Fe_2{}^{3+}(PO4)_2(OH)_2$ – Implications for the molecular structure. Journal of Molecular Structure, 1051, 292-298.

Frost, R.L., Xi, Y., Millar, G., Tan, K., and Palmer, S.J. (2013b) Vibrational spectroscopy of natural cave mineral monetite CaHPO4 and the synthetic analog. Spectroscopy Letters, 46(1), 54-59.

Frost, R.L., Xi, Y., Scholz, R., and Belotti, F.M. (2013c) Vibrational spectroscopic characterization of the phosphate mineral ludlamite $(Fe,Mn,Mg)_3(PO_4)_2 \cdot 4H_2O$–A mineral found in lithium bearing pegmatites. Spectrochimica Acta Part A: Molecular and Biomolecular Spectroscopy, 103, 143-150.

Gagné, O.C., and Hawthorne, F.C. (2018) Bond-length distributions for ions bonded to oxygen: Results for the non-metals and discussion of lone-pair stereoactivity and the polymerization of PO_4. Acta Crystallographica Section B: Structural Science, Crystal Engineering and Materials, 74(1), 79-96.

Gellert, R., Rieder, R., Brückner, J., Clark, B., Dreibus, G., Klingelhöfer, G., Lugmair, G., Ming, D., Wänke, H., and Yen, A. (2006) Alpha Particle X-ray Spectrometer (APXS): Results from Gusev crater and calibration report. Journal of Geophysical Research: Planets, 111, E02S05.

Goetz, W., Bertelsen, P., Binau, C.S., Gunnlaugsson, H.P., Hviid, S.F., Kinch, K.M., Madsen, D.E., Madsen, M.B., Olsen, M., and Gellert, R. (2005) Indication of drier periods on Mars from the chemistry and mineralogy of atmospheric dust. Nature, 436(7047), 62-65.

Gonçalve , R., Martins, R., Costa, C.M., Ferdov, S., and Lanceros-Méndez, S. (2017) Crystal Morphology Control of Synthetic Giniite by Alkaline Cations and pH Variations. Crystal Growth & Design, 17(9), 4710-4714.

Grotzinger, J.P., Sumner, D.Y., Kah, L., Stack, K., Gupta, S., Edgar, L., Rubin, D., Lewis, K., Schieber, J., and Mangold, N. (2014) A habitable fluvio-lacustrine environment at Yellowknife Bay, Gale Crater, Mars. Science, 343(6169), 1242777.

Han, C., Zhoumin, Ye, Q., Yao, L., and Xu, Z. (2017) Controllable synthesis of sphere-and star-like $Fe_5(PO_4)_4(OH)_3 \cdot 2H_2O$ microcrystals for effective photo-Fenton-like degradation of rhodamine B. Inorganic and Nano-Metal Chemistry, 47(6), 806-809.

Hausrath, E.M., and Tschauner, O. (2013) Natural fumarolic alteration of fluorapatite, olivine, and basaltic glass, and implications for habitable environments on Mars. Astrobiology, 13(11), 1049-1064.

Hausrath, E., Golden, D., Morris, R., Agresti, D., and Ming, D. (2013) Acid sulfate alteration of fluorapatite, basaltic glass and olivine by hydrothermal vapors and fluids: Implications for fumarolic activity and secondary phosphate phases in sulfate-rich Paso Robles soil at Gusev Crater, Mars. Journal of Geophysical Research: Planets, 118, 1-13.

Hausrath, E. M., Ming, D. W., Peretyazhko, T., and Rampe, E.B., (2018) Reactive transport and mass balance modeling of the Stimson sedimentary formation and altered fracture zones constrain diagenetic conditions at Gale crater, Mars. Earth and Planetary Science Letters, 491, 1-10.

Hawthorne, F.C. (1998) Structure and chemistry of phosphate minerals. Mineralogical Magazine, 62(2), 141-164.

Hong, Y.S., Ryu, K.S., and Chang, S.H. (2003) New Iron-Containing Electrode Materials for Lithium Secondary Batteries. Electronics and Telecommunications Research Institute Journal, 25(5), 412-417.

Hurowitz, J.A., McLennan, S., Tosca, N., Arvidson, R., Michalski, J.R., Ming, D.W., Schroder, C., and Squyres, S.W. (2006) In situ and experimental evidence for acidic weathering of rocks and soils on Mars. Journal of Geophysical Research, 111, E02S19.

Jambor, J., and Dutrizac, J. (1988) Synthesis of the ferric analog of the ferrous-ferric phosphate, giniite. Neues Jahrbuch für Mineralogie / Abhandlungen, 159(1), 51-58.

Jones, R.H., McCubbin, F.M., Dreeland, L., Guan, Y., Burger, P.V., and Shearer, C.K. (2014) Phosphate minerals in LL chondrites: A record of the action of fluids during metamorphism on ordinary chondrite parent bodies. Geochimica et Cosmochimica Acta, 132, 120-140.

Kanowitz, S.M., and Palenik, G.J. (1998) Bond Valence Sums in Coordination Chemistry Using Oxidation-State-Independent R 0 Values. A Simple Method for Calculating the Oxidation State of Iron in Fe− O Complexes. Inorganic Chemistry, 37(8), 2086-2088.

Keller, P. (1980a) GINIIT, $Fe^{2+}Fe_4^{3+}((H_2O)_2(OH)_2(PO_4)_4)$, Ein Neues Mineral Aus Dem Pegmatit von Sandamab Bei Usakos, Namibia. Neues Jahrbuch für ineralogie. /Monatshefte, 2, 49-56.

-. (1980b) GINIT, Fe^{2+} Fe_4^{3+} $((H_2O)_2(OH)_2(PO_4)_4)$: Neue Kristallographische Daten. Neues Jahrbuch fü Mineralogie / Monatshefte, 12, 561-563.

Keller, P., and Knorring, O. (1989) Pegmatites at the Okatjimukuju farm, Karibib, Namibia Part I: Phosphate mineral associations of the Clementine II pegmatite. European Journal of Mineralogy, 567-594.

Klingelhöfer, G., Morris, R.V., Bernhardt, B., Schröder, C., Rodionov, D.S., De Souza, P., Yen, A., Gellert, R., Evlanov, E., and Zubkov, B. (2004) Jarosite and hematite at Meridiani Planum from Opportunity's Mössbauer spectrometer. Science, 306(5702), 1740-1745.

Kolesov, B. (2006) Raman investigation of H_2O molecule and hydroxyl groups in the channels of hemimorphite. American Mineralogist, 91(8-9), 1355-1362.

Lafuente, B., Downs, R.T., Yang, H., and Stone, N. (2016) The power of databases: the RRUFF project. In A. T, and D.R. M, Eds. Highlights in mineralogical crystallography, p. 1-29. Walter de Gruyter GmbH, Berlin.

Liu, A., Ma, F., and Chen, Y. (2017) Synthesis of shape-controlled $Fe_5(PO_4)_4(OH)_3 \cdot 2H_2O$ microcrystal via one-step hydrothermal method. Micro & Nano Letters, 12(5), 325-328.

Lv, C., Duan, X., Deng, J., and Wang, T. (2017) LiFePO 4 mesocrystals coated with N-doped carbon from an ionic liquid for Li-ion batteries. CrystEngComm, 19(9), 1253-1257.

Martins, P., Salazar, H., Aoudjit, L., Gonçalves, R., Zioui, D., Fidalgo-Marijuan, A., Costa, C., Ferdov, S., and Lanceros-Mendez, S. (2020) Crystal morphology control of synthetic giniite for enhanced photo-Fenton activity against the emerging pollutant metronidazole. Chemosphere, 128300.

McCollom, T.M., Donaldson, C., Moskowitz, B., Berquó, T.S., and Hynek, B. (2018) Phosphorous immobility during formation of the layered sulfate deposits of the Burns formation at Meridiani Planum. Journal of Geophysical Research: Planets, 123(5), 1230-1254.

McCubbin, F.M., and Jones, R.H. (2015) Extraterrestrial apatite: Planetary geochemistry to astrobiology. Elements, 11(3), 183-188.

McCubbin, F.M., Jolliff, B.L., Nekvasil, H., Carpenter, P.K., Zeigler, R.A., Steele, A., Elardo, S.M., and Lindsley, D.H. (2011) Fluorine and chlorine abundances in lunar apatite: Implications for heterogeneous distributions of magmatic volatiles in the lunar interior. Geochimica et Cosmochimica Acta, 75(17), 5073-5093.

McCubbin, F.M., Shearer, C.K., Burger, P.V., Hauri, E.H., Wang, J., Elardo, S.M., and Papike, J.J. (2014) Volatile abundances of coexisting merrillite and apatite in the martian meteorite Shergotty: Implications for merrillite in hydrous magmas. American Mineralogist, 99(7), 1347-1354.

McGowan, G., and Prangnell, J. (2006) The significance of vivianite in archaeological settings. Geoarchaeology: An International Journal, 21(1), 93-111.

McSween, H., and Treiman, A. (1998) Planetary Materials. Reviews in Mineralogy, 36, 6-1.

Miller, H.M., Mayhew, L.E., Ellison, E.T., Kelemen, P., Kubo, M., and Templeton, A.S. (2017) Low temperature hydrogen production during experimental hydration of partially-serpentinized dunite. Geochimica et Cosmochimica Acta, 209, 161-183.

Ming, D.W., Mittlefehldt, D.W., Morris, R.V., Golden, D., Gellert, R., Yen, A., Clark, B.C., Squyres, S.W., Farrand, W.H., and Ruff, S.W. (2006) Geochemical and mineralogical indicators for aqueous processes in the Columbia Hills of Gusev crater, Mars. Journal of Geophysical Research: Planets, 111, E02S12.

Mojzsis, S.J., and Arrhenius, G. (1998) Phosphates and carbon on Mars: exobiological implications and sample return considerations. Journal of Geophysical Research: Planets, 103(E12), 28495-28511.

Mojzsis, S.J., Arrhenius, G., McKeegan, K., Harrison, T., Nutman, A., and Friend, C. (1996) Evidence for life on Earth before 3,800 million years ago. Nature, 384(6604), 55-59.

Moore, P. (1973) Pegmatite phosphates: descriptive mineralogy and crystal chemistry. Mineralogical Record, 4(3), 103-130.

Morris, R.V., Klingelhoefer, G., Schröder, C., Rodionov, D.S., Yen, A., Ming, D.W., De Souza, P., Wdowiak, T., Fleischer, I., and Gellert, R. (2006) Mössbauer mineralogy of rock, soil,

and dust at Meridiani Planum, Mars: Opportunity's journey across sulfate-rich outcrop, basaltic sand and dust, and hematite lag deposits. Journal of Geophysical Research: Planets, 111(E12).

Morris, R.V., Ming, D., Blake, D., Vaniman, D., Bish, D., Chipera, S., Downs, R., Gellert, R., Treiman, A., Yen, A., and others and the MSL Science Team (2013) The amorphous component in martian basaltic soil in global perspective from MSL and MER missions. In LPI, Ed. 44th Lunar and Planetary Science conference, p. 1653. LPI, The Woodlands, TX.

Nedkov, I., Groudeva, V., Angelova, R., Iliev, M., and Slavov, L. (2016) New Iron Oxides/Hydroxides Biomaterials for Application in Electronics and Medicine. Machines. Technologies. Materials., 10(12), 48-51.

Nunes, A.P.L., de Araujo, A.C., de Magalhães, P.R., and Viana, A.B.H. (2009) Occurence of phosphorus-bearing minerals in Brazilian iron ores. Proceedings of the GEOMIN 2009 Conference, First International Seminar on Geology for the Mining Industry, p. 10-12, Antofagasta, Chile.

Ofoegbu, S.U. (2019) Technological challenges of phosphorus removal in high-phosphorus ores: Sustainability implications and possibilities for greener ore processing. Sustainability, 11(23), 6787.

Pasek, M.A., and Kee, T.P. (2011) On the origin of phosphorylated biomolecules. In R. Egel, Lankenau, D., Mulkidjanian, A.Y. , Ed. Origins of Life: The Primal Self-Organization, p. 57-84. Springer, Berlin, Heidelberg.

Patiño Douce, A.E., Roden, M.F., Chaumba, J., Fleisher, C., and Yogodzinski, G. (2011) Compositional variability of terrestrial mantle apatites, thermodynamic modeling of

apatite volatile contents, and the halogen and water budgets of planetary mantles. Chemical Geology, 288(1), 14-31.

Poienar, M., Damay, F., Rouquette, J., Ranieri, V., Malo, S., Maignan, A., Elkaïm, E., Haines, J., and Martin, C. (2020) Structural and magnetic characterization of barbosalite $Fe_3(PO_4)_2(OH)_2$. Journal of Solid State Chemistry, 121357.

Powner, M.W., Gerland, B., and Sutherland, J.D. (2009) Synthesis of activated pyrimidine ribonucleotides in prebiotically plausible conditions. Nature, 459(7244), 239-242.

Priambodo, R., Tan, Y.-L., Shih, Y.-J., and Huang, Y.-H. (2017) Fluidized-bed crystallization of iron phosphate from solution containing phosphorus. Journal of the Taiwan Institute of Chemical Engineers, 80, 247-254.

Rampe, E.B., Morris, R.V., Archer, P.D., Agresti, D.G., and Ming, D.W. (2016) Recognizing sulfate and phosphate complexes chemisorbed onto nanophase weathering products on Mars using in-situ and remote observationsk. American Mineralogist, 101(3), 678-689.

Rampe, E., Ming, D., Blake, D., Bristow, T., Chipera, S., Grotzinger, J., Morris, R., Morrison, S., Vaniman, D., and Yen, A. (2017) Mineralogy of an ancient lacustrine mudstone succession from the Murray formation, Gale crater, Mars. Earth and Planetary Science Letters, 471, 172-185.

Rampe, E.B., Blake, D.F., Bristow, T., Ming, D.W., Vaniman, D., Morris, R., Achilles, C., Chipera, S., Morrison, S., and Tu, V. (2020) Mineralogy and geochemistry of sedimentary rocks and eolian sediments in Gale crater, Mars: A review after six Earth years of exploration with Curiosity. Geochemistry, 80(2), 125605.

Redhammer, G., Tippelt, G., Roth, G., Lottermoser, W., and Amthauer, G. (2000) Structure and Mössbauer spectroscopy of barbosalite $Fe^{2+}Fe^{3+}{}_2(PO_4)_2(OH)_2$ between 80 K and 300 K. Physics and Chemistry of Minerals, 27(6), 419-429.

Roncal-Herrero, T., Rodríguez-Blanco, J.D., Benning, L.G., and Oelkers, E.H. (2009) Precipitation of iron and aluminum phosphates directly from aqueous solution as a function of temperature from 50 to 200 C. Crystal Growth & Design, 9(12), 5197-5205.

Rouzies, D., Varloud, J., and Millet, J.-M.M. (1994) Thermal behaviour and physico-chemical characterization of synthetic and natural iron hydroxyphosphates. Journal of the Chemical Society, Faraday Transactions, 90(21), 3335-3339.

Sanders, G.B., and Larson, W.E. (2011) Integration of in-situ resource utilization into lunar/Mars exploration through field analogs. Advances in Space Research, 47(1), 20-29.

Shearer, C.K., Hess, P.C., Wieczorek, M.A., Pritchard, M.E., Parmentier, E.M., Borg, L.E., Longhi, J., Elkins-Tanton, L.T., Neal, C.R., and Antonenko, I. (2006) Thermal and magmatic evolution of the Moon. Reviews in Mineralogy and Geochemistry, 60(1), 365-518.

Shearer, C., Burger, P., Papike, J., McCubbin, F., and Bell, A. (2015) Crystal chemistry of merrillite from Martian meteorites: Mineralogical recorders of magmatic processes and planetary differentiation. Meteoritics & Planetary Science, 50(4), 649-673.

Sheldrick, G.M. (2015a) Crystal structure refinement with SHELXL. Acta Crystallographica Section C: Structural Chemistry, 71(1), 3-8.

-. (2015b) SHELXT–Integrated space-group and crystal-structure determination. Acta Crystallographica Section A: Foundations and Advances, 71(1), 3-8.

Sridhar, K., Finn, J., and Kliss, M. (2000) In-situ resource utilization technologies for Mars life support systems. Advances in Space Research, 25(2), 249-255.

Starr, S.O., and Muscatello, A.C. (2020) Mars in situ resource utilization: a review. Planetary and Space Science, 182, 104824.

Taylor, G.J. (2013) The bulk composition of Mars. Geochemistry, 73(4), 401-420.

Treiman, A., Downs, R., Ming, D., Morris, R., Thorpe, M., Hazen, R., Downs, G., Rampe, E., and CheMin Team, T. (2021) Possible Detection of a Jahnsite-Whiteite Group Phosphate Mineral by MSL CheMin in Glen Torridon, Gale Crater, Mars. 52nd Lunar and Planetary Science Conference, p. 1200. LPI, Virtual.

Tu, V.M., Hausrath, E.M., Tschauner, O., Iota, V., and Egeland, G.W. (2014) Dissolution rates of amorphous Al-and Fe-phosphates and their relevance to phosphate mobility on Mars. American Mineralogist, 99(7), 1206-1215.

Ullrich, B. (2018) Zur Mineralogie anthropogen induzierter Alterationsprozesse–Sekundärminerale des historischen Alaunschieferbergbaus von Saalfeld und Schmiedefeld im Thüringischen Schiefergebirge. Geologica Saxonica, 64, 67-79.

Vaniman, D., Bish, D., Ming, D., Bristow, T., Morris, R., Blake, D., Chipera, S., Morrison, S., Treiman, A., and Rampe, E. (2014) Mineralogy of a mudstone at Yellowknife Bay, Gale crater, Mars. Science, 343(6169), 1243480.

Wald, G. (1964) The origins of life. Proceedings of the National Academy of Sciences of the United States of America, 52(2), 595.

Wänke, H., and Dreibus, G. (1988) Chemical composition and accretion history of terrestrial planets. Philosophical Transactions of the Royal Society of London. Series A, Mathematical and Physical Sciences, 325(1587), 545-557.

Weber, I., Böttger, U., Pavlov, S.G., Stojic, A., Hübers, H.W., and Jessberger, E.K. (2018) Raman spectra of hydrous minerals investigated under various environmental conditions in preparation for planetary space missions. Journal of Raman Spectroscopy, 49(11), 1830-1839.

Weckwerth, G., and Schidlowski, M. (1995) Phosphorus as a potential guide in the search for extinct life on Mars. Advances in Space Research, 15(3), 185-191.

Westheimer, F.H. (1987) Why nature chose phosphates. Science, 235(4793), 1173-1178.

Whittingham, M.S. (2004) Lithium batteries and cathode materials. Chemical Reviews, 104(10), 4271-4302.

Wiseman, S.M., Arvidson, R., Andrews-Hanna, J., Clark, R., Lanza, N., Des Marais, D., Marzo, G., Morris, R., Murchie, S., and Newsom, H.E. (2008) Phyllosilicate and sulfate-hematite deposits within Miyamoto crater in southern Sinus Meridiani, Mars. Geophysical Research Letters, 35(19).

Yang, H., Sun, H.J., and Downs, R.T. (2011) Hazenite, KNaMg2 (PO4) 2· 14H2O, a new biologically related phosphate mineral, from Mono Lake, California, USA. American Mineralogist, 96(4), 675-681.

Yang, X., and Post, W.M. (2011) Phosphorus transformations as a function of pedogenesis: A synthesis of soil phosphorus data using Hedley fractionation method. Biogeosciences, 8(10), 2907.

Yen, A., Ming, D., Vaniman, D., Gellert, R., Blake, D., Morris, R., Morrison, S., Bristow, T., Chipera, S., and Edgett, K. (2017) Multiple stages of aqueous alteration along fractures in mudstone and sandstone strata in Gale Crater, Mars. Earth and Planetary Science Letters, 471, 186-198.

Zhang, S.M., Zhang, J.X., Xu, S.J., Yuan, X.J., and Tan, T. (2013) Synthesis, morphological analysis and electrochemical performance of iron hydroxyl phosphate as a cathode material for lithium ion batteries. Journal of Power Sources, 243, 274-279.

Figure Captions

Figure 1. BSE image at 15 kV of giniite. Dots are locations of EMP analysis on the crystal.

Figure 2. Calculated comparison of XRD patterns of natural (top and bottom patterns) and synthetic ferrian (middle pattern) giniite. Patterns are calculated for Cu*Kα* radiation.

Figure 3. Broad Scan Raman spectra of giniite showing band consistent with giniite chemistry and structure. Typical PO4, Fe-O, and O-H ranges are shown at bottom of figure and are consistent with Raman of synthetic giniite and other minerals with structure similarities. 2nd-order Savitzky-Golay filter applied (interval of 10). See Supplementary Figure S2 for plot of raw data.

Figure 4. Giniite structure viewed down *b* (top) and *a* (bottom) axes. Four unit cells pictured. Spheres on tetrahedral and octahedral corners are oxygen. Smaller spheres are H^+. O7 oxygen atoms discussed in the text are labeled in lower right cell of the top panel. Supplementary Figure S3 is a close up of this "void" area.

Tables

Table 1. Summary of crystallographic data for giniite

Empirical chemical formula	$(Fe^{2+}_{0.80}Mn_{0.11}Mg_{0.02})_{\Sigma=0.93}Fe^{3+}_{4}(PO_4)_{4.03}(OH)_2 \cdot 2H_2O$
Ideal chemical formula	$Fe^{2+}Fe^{3+}_{4}(PO_4)_4(OH)_2 \cdot 2H_2O$
Crystal symmetry	Monoclinic
Space group	*P*2/*n*
a (Å)	10.3472(6)
b (Å)	5.1497(2)
c (Å)	14.2338(7)
β (°)	111.175(6)
V(Å^3)	707.24(7)

Table 2. Select bond distances (Å) for giniite

Fe1—O8	1.986 (2)	P1—O3	1.518 (2)
Fe1—O7	2.069 (2)	P1—O1	1.526 (2)
Fe1—O2	2.082 (2)	P1—O4	1.544 (2)
Fe1—O10W	2.183 (2)	P1—O2	1.553 (2)
Fe1—O4	2.253 (2)	Ave.	1.54 (2)
Fe1—O9H	2.279 (2)		
Ave.	2.14 (12)		
		P2—O6	1.513 (2)
Fe2—O4 x 2	1.995 (2)	P2—O5	1.521 (2)
Fe2—O2 x 2	2.013 (2)	P2—O8	1.537 (2)
Fe2—O9H x 2	2.024 (2)	P2—O7	1.563 (2)
Ave.	2.01 (2)	Ave.	1.53 (2)
Fe3—O6	1.938 (2)		
Fe3—O5	1.954 (2)		
Fe3—O3	1.969 (2)		
Fe3—O1	1.985 (2)		
Fe3—O9H	2.024 (2)		
Fe3—O10W	2.226 (2)		
Ave.	2.02 (11)		

Table 3. Bond Valence calculations for Fe-O and P-O bonds.

	Fe1	Fe2	Fe3	P1	P2	Sum
O1			0.543	1.323		1.866
O2	0.356	0.503 x 2↓		1.233		2.092
O3			0.567	1.354		1.920
O4	0.224	0.529 x 2↓		1.263		2.016
O5			0.591		1.341	1.932
O6			0.617		1.373	1.990
O7	0.369				1.199	**1.568**
O8	0.462				1.287	1.749
O9	0.209	0.489 x 2↓	0.489			1.187
O10	0.271		0.283			0.554
Sum	1.891	3.042	3.090	5.173	5.200	

Table 4. Comparison of chemical analyses of giniite by EMP in oxide wt%. This study compared to Keller (1980a).

	Analysis			***Fitted***[d]			
(wt%)	***Keller***	***This Study***[b]		***Keller***	***This Study Ideal***	***This Study Best Fit***	***Ideal***
Fe_2O_3	46.07	51.25	(0.34)	39.21	42.74	41.73	43.80
FeO	-	-	-	6.17	7.66	8.57	9.85
Al_2O_3	1.20	-	-	1.20			
MgO	0.68	0.10	(0.02)	0.68	0.10	0.10	
P_2O_5	36.99	38.34	(0.25)	36.99	38.34	38.34	38.94
MnO	0.63	1.07	(0.20)	0.63	1.07	1.07	
$H_2O_{(Total)}$[a]	-	-	-	6.95	7.24	7.31	7.41
Total	85.57	90.76	(0.37)	91.83	97.15	97.11	100.00

NOTE: Parenthetical values are 1 standard deviation. [a]$H_2O_{(Total)}$ is the wt% sum of OH^- and molecular H_2O. [b]Based on 15 analyses. [d]Values in table are based on a calculated fit. Fits for Keller and "This Study Ideal" based on ideal formula and fully occupied Fe^{3+} sites. "This Study Best Fit" represent best fit result from a range of calculated stoichiometries using EMP data from this study.

Figures

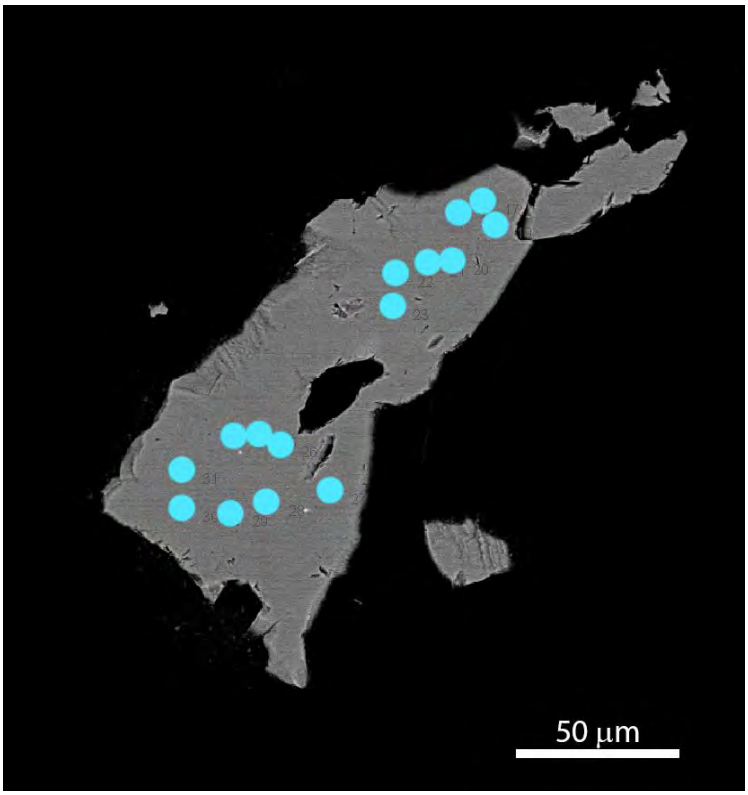

Figure 1. BSE image at 15 kV of giniite. Dots as locations of EMP analysis on the crystal.

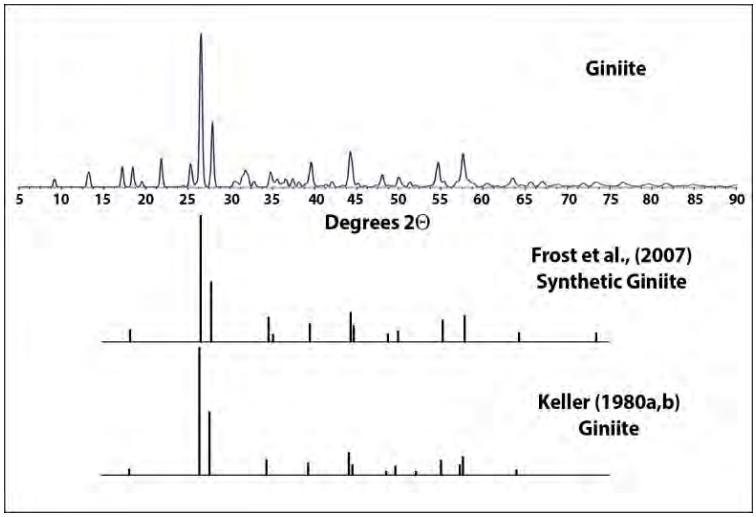

Figure 2. Calculated comparison of XRD patterns of natural (top and bottom patterns) and synthetic ferrian (middle pattern) giniite. Patterns are calculated for Cu*Kα* radiation.

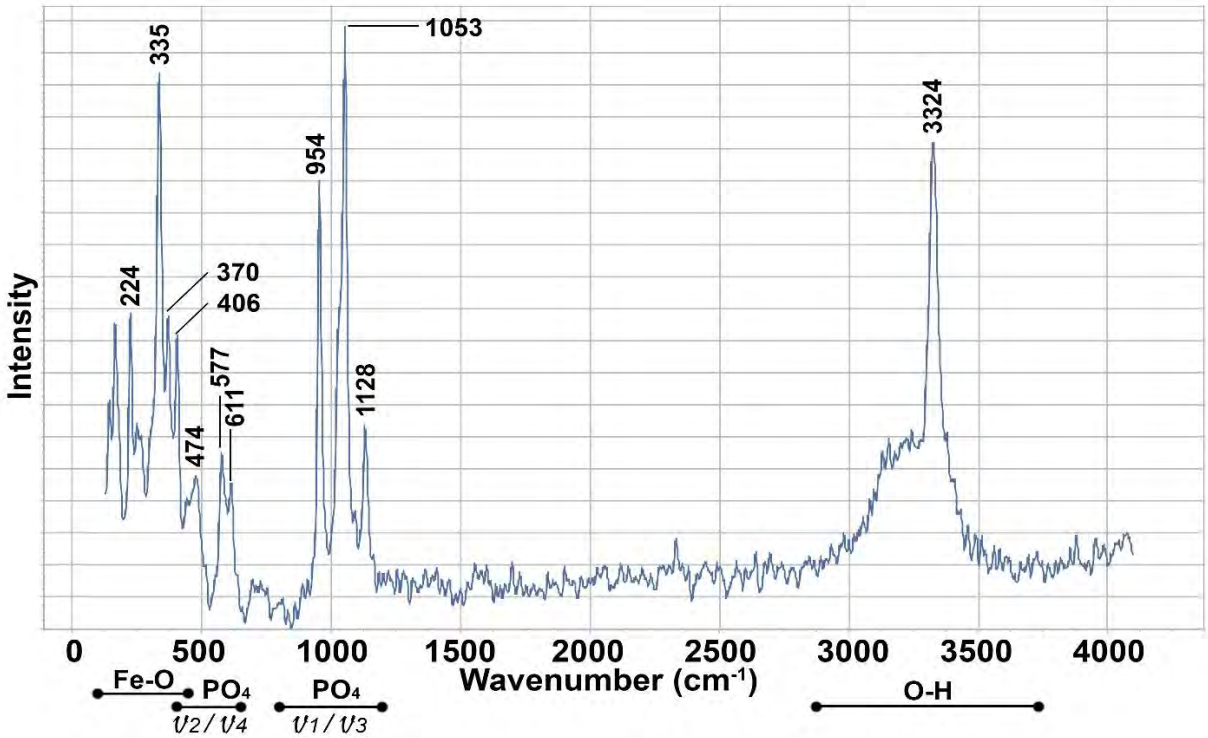

Figure 3. Broad Scan Raman spectra of giniite showing band consistent with giniite chemistry and structure. Typical PO4, Fe-O, and O-H ranges are shown at bottom of figure and are consistent with Raman of synthetic giniite and other minerals with structure similarities. 2nd-order Savitzky-Golay filter applied (interval of 10). See Supplementary Figure S2 for plot of raw data.

This is the peer-reviewed, final accepted version for American Mineralogist, published by the Mineralogical Society of America.
The published version is subject to change. Cite as Authors (Year) Title. American Mineralogist, in press.
DOI: https://doi.org/10.2138/am-2022-8138. http://www.minsocam.org/

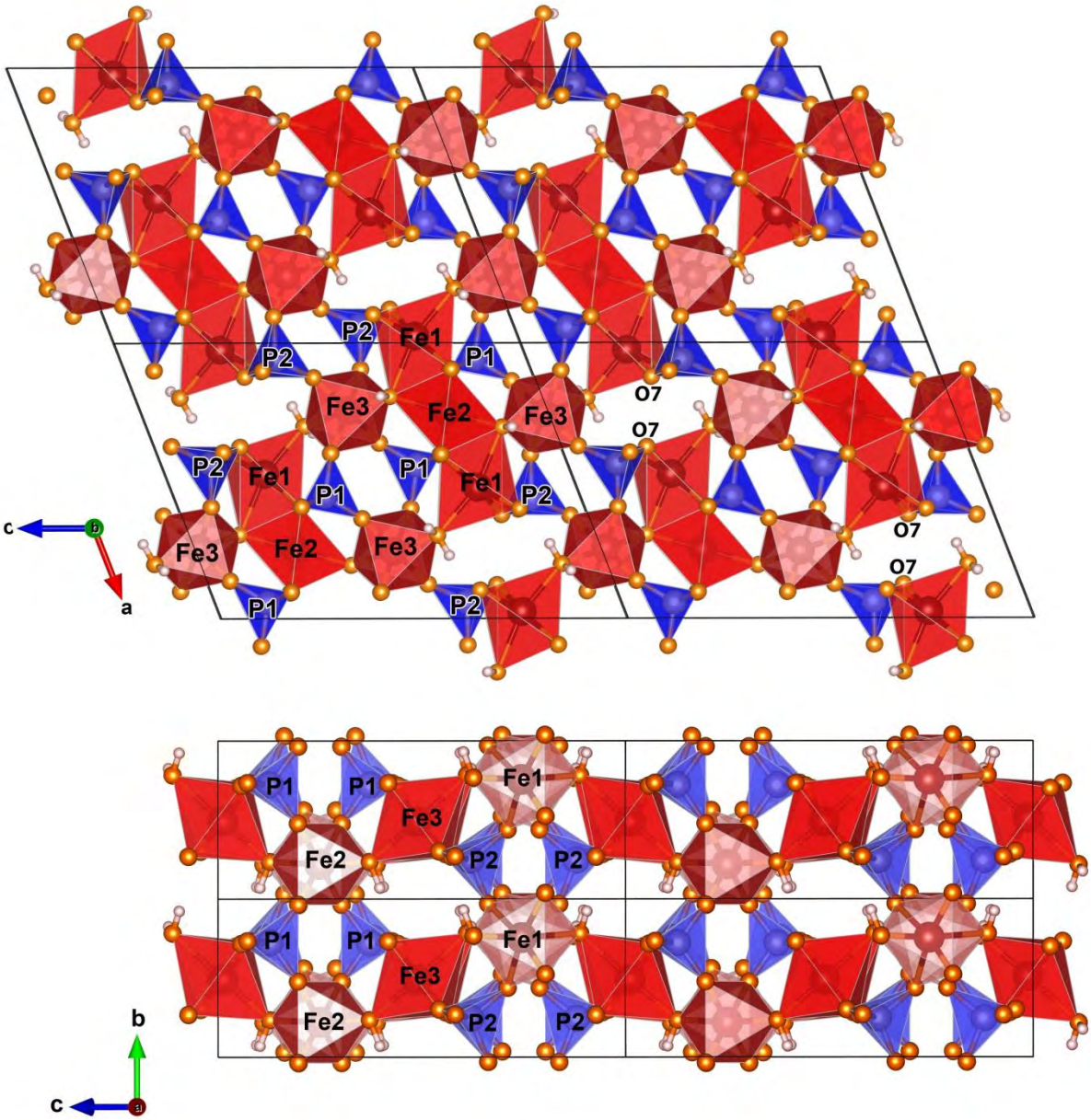

Figure 4. Giniite structure viewed down *b* (top) and *a* (bottom) axes. Four unit cells pictured. Spheres on tetrahedral and octahedral corners are oxygen. Smaller spheres are H^+. O7 oxygen atoms discussed in the text are labeled in lower right cell of the top panel. Supplementary Figure S3 is a close up of this "void" area.